Journal of ELECTRONIC MATERIALS, Vol. 47, No. 9, 2018
https://doi.org/10.1007/s11664-018-6144-6

TOPICAL COLLECTION: 17TH CONFERENCE ON DEFECTS (DRIP XVII)

Catastrophic Optical Damage of GaN-Based Diode Lasers: Sequence of Events, Damage Pattern, and Comparison with GaAs-Based Devices

JENS W. TOMM,[1,5] ROBERT KERNKE,[1] GIOVANNA MURA,[2] MASSIMO VANZI,[2] MARTIN HEMPEL,[3] and BRUNO ACKLIN[4]

1.—Max-Born-Institut für Nichtlineare Optik und Kurzzeitspektroskopie, Max Born Str. 2A, 12489 Berlin, Germany. 2.—Department of Electrical and Electronic Engineering, University of Cagliari, 09124 Cagliari, Italy. 3.—Fraunhofer IZM, Gustav-Meyer-Allee 25, 13355 Berlin, Germany. 4.—Mountain View, CA 94040, USA. 5.—e-mail: tomm@mbi-berlin.de

Gallium-nitride-based diode lasers were intentionally damaged using single sub-μs current pulses. This approach provoked catastrophic optical damage, a known sudden degradation mechanism, which becomes evident as surface modification at the aperture, where the 450-nm laser emission leaves the waveguide of the device. Subsequently, we analyzed the related damage pattern inside the device. Knowledge about the operating conditions, degradation time, and energy introduced into the defect allows estimates of the temperature during the process ($\sim$ 1000°C) and defect propagation velocity (110 μm/μs). Further analysis of this data allows for conclusions regarding the mechanisms that govern defect creation at the surface and defect propagation inside the device. Moreover, we compared these findings with earlier results obtained from gallium-arsenide-based devices and find similarities in the overall scenario, while the defect initialization and defect pattern are strikingly different.

Key words: Catastrophic optical damage, COD, GaN-based diode laser, generic degradation, damage pattern

INTRODUCTION

Gallium nitride (GaN)-based light-emitting diodes and diode lasers represent an enabling technology affecting all of society. While their performance has undergone tremendous improvements, laser power levels achieved so far still fall short of those of their GaAs-based infrared-emitting counterparts. This explains why, up to now, effects typical for high-power operation, e.g., catastrophic optical damage (COD), have not attracted broad attention in literature on GaN-based diode lasers.

COD is a generic degradation effect related to high power density and cannot be eliminated, but only deferred towards higher photon density. Thus, its microscopic understanding is of fundamental interest, far beyond failure analysis, which might be restricted to a specific device design or even specific operation conditions. COD has been extensively studied for GaAs-based diode lasers (see references in reviews[1,2]). There are, however, reports on observation of COD in GaN-based devices, as well.[3–10]

We present herein results of analysis of damage patterns created by COD in GaN-based devices. The creation sequence of the defects is discussed, and mechanisms of defect propagation are analyzed. Finally, we compare these findings with earlier results obtained for GaAs-based devices.

EXPERIMENTAL PROCEDURES

We investigated 450-nm-emitting PL TB450B devices in TO56 package from Osram. These devices are based on a multiple quantum well (MQW) as

(Received November 8, 2017; accepted February 13, 2018; published online February 26, 2018)

gain medium, a GaN-based waveguide, and AlGaN claddings. The n- and p-claddings are silicon and magnesium doped, respectively. The emitter stripe width is 15 μm, and the cavity length is 1.2 mm. The threshold current is $\sim$ 200 mA. A batch of 16 devices were subjected to single-pulse step tests, as introduced earlier for GaAs-based devices.[11] Except for one, all devices showed a damage pattern at the front facet, very similar to that reported in Refs. 3,7, and 12. The particular device whose data are exemplarily presented here showed COD within a single 800-ns current pulse at $\sim$ 5 A. Comparing the shape of the power transients taken before and during COD, the "missing energy" in the single COD pulse was determined.[10] We estimated a value of 2 ± 1 μJ, and assume this to be the amount introduced into the damaged site.

Scanning electron microscopy (SEM), scanning transmission electron microscopy (STEM) observations, and focused ion beam (FIB) preparation were implemented using an FEI Dual-Beam Nova Nanolab 600 system. The instrument used for TEM/STEM was a FEI Tecnai F20 ST, operated at 200 keV. Lamellas were extracted from the center of the active region of the device. Thus, the lamellas represent planes spanned by the laser axis and growth direction. In this way, the damage pattern in the active region, MQW, and waveguide become visible from the side.

RESULTS

Figure 1 shows the damage pattern as seen from two FIB lamellas extracted from the active region. The damage appears as an empty channel with dimensions of $\sim$ 80 μm (length along lasing axis), $\sim$ 400 nm (height), and 6.5 μm (width). The first two values were taken directly from the SEM images shown in Fig. 1, while the width was estimated from SEM images taken from the front facet (not shown here) (see, e.g., Ref. 7). Taking into account these dimensions, the volume of the empty channel is 2.1×10^{-10} cm^{-3}. Assuming an average density $\rho = 6.15$ g/cm^3 for the active region material, the mass of material that originally filled this volume was 1.3×10^{-9} g.

Figure 2 provides details on the very end of the channel with the highest spatial resolution achieved. Interestingly, the MQW in front of the channel are well visible, especially on the thinner, tilted interface inside the 20-nm-wide lamella section, and they appear undisturbed. From this, we conclude that there is virtually no transition region between the undisturbed MQWs in front and the empty channel behind. Taking the MQW layers as reference, more pronounced extension of the channel is observed towards the n- (bottom) than p-side (top), indicating an asymmetric waveguide design.

DISCUSSION

Damage Pattern and Temperatures

The position of the damage pattern within the sequence of the epitaxial layers exactly matches the expected position of the optical mode (Fig. 2). This is consistent with the assumption that the propagation of the COD-related damage front is fed and controlled by laser radiation.[2] This provides an argument that COD in GaN-based devices is based on the same mechanisms as in GaAs-based lasers. The appearance of the damage pattern, however, is somewhat surprising, because of the lack of any disordered material. The channel does not show any transition region towards unaffected material down to the dimension of a few nanometers. An empty channel is well consistent with the material loss that has been detected during COD in GaN-based devices. Hempel et al.[12] visualized this material loss using a thermocamera synchronized to the COD event provoked by a single pulse, as well.

In addition to the size of the empty channel, we can estimate the energy introduced into the defect from the output power missing during the pulse that provoked the catastrophic damage. Using the specific heat capacity of GaN and assuming that all the missing energy was confined only to the affected zone, i.e., neglecting scattering and lateral heat

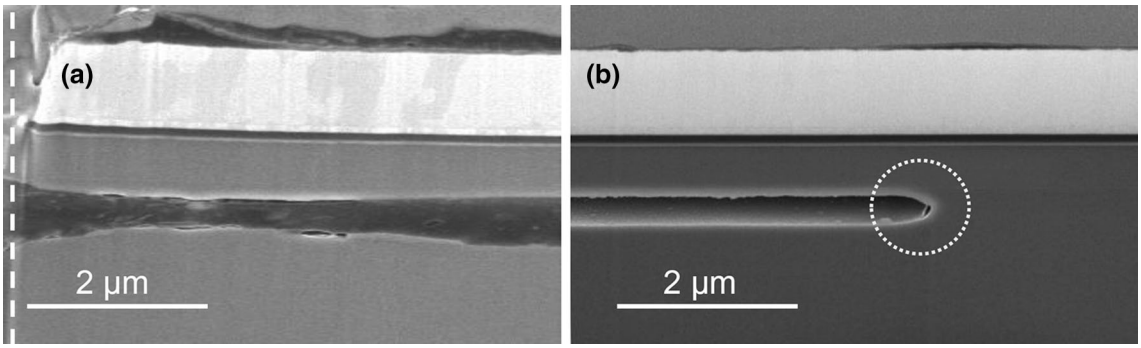

Fig. 1. (a) First section of channel created by COD starting at front facet; see dashed vertical line on the left. (b) Final section of the channel, which has length of $\sim$ 80 μm. The figures are SEM images taken from FIB lamellas extracted from the device starting at the front facet. Bright regions on top of the images are p-metallizations defining the emitter stripes. Dotted circle marks the very end of the channel.

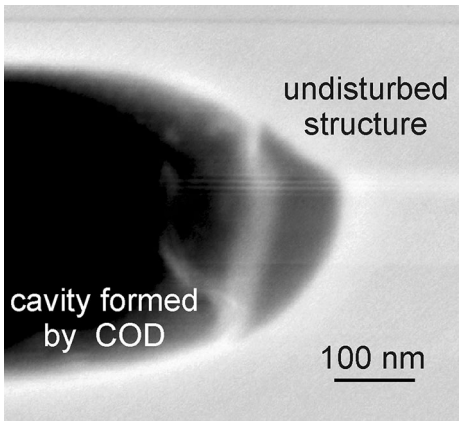

Fig. 2. STEM image of part of FIB lamella at end of channel; see the region marked by the dotted circle in Fig. 1b. The MQW layers are clearly resolved.

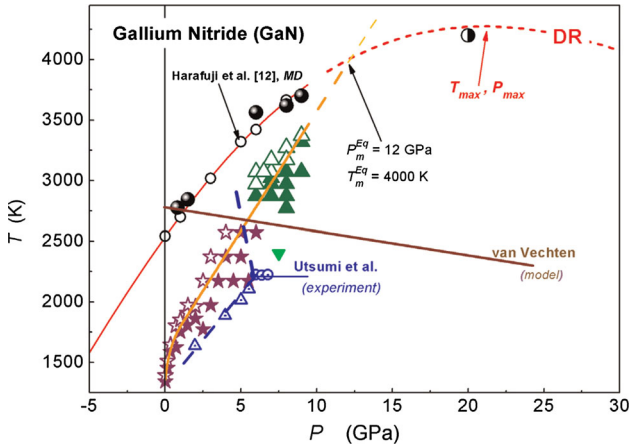

Fig. 3. Pressure dependence of GaN melting and decomposition in *P–T* phase diagram, reproduced with permission from Ref. 13. Melting is described by the red curve labeled DR, while the data that describe the decomposition behavior as experimentally determined by Utsumi et al.[14] are connected by a blue dashed line (Color figure online).

diffusion during the < 800 ns event, one can estimate an upper limit of 3500 K for the temperature rise.[7] The effective temperature rise during the COD process is probably substantially lower, because of light scattering and heat diffusion into the surrounding material.

In GaN, material alterations begin substantially below the melting point of ~ 2500°C (see the phase diagram in Fig. 3 reproduced from Ref. 13). In contrast to gallium, aluminum, and arsenic, nitrogen is gaseous at ambient temperature. Its vapor pressure in GaN crystal exceeds 0.1 MPa (ambient pressure) as the temperature reaches ~ 1000°C, leading to disintegration of the crystal well before the actual melting point is reached. Disintegration of the (for 450-nm light transparent) semiconductor is expected to increase the absorption of the remaining material. This is expected to start the COD mechanism.

Pressures of several GPa are required to measure the "regular" melting point of ~ 2500°C (see Table I). Therefore, N_2 expansion is the likely cause of the observed material ejection[12] from the COD channel. The higher melting point of AlN of 4800 K, associated with lower nitrogen pressure at temperatures between ambient and 1000°C, may represent the explanation for the abrupt interface between the evaporated GaN waveguide and undisturbed cladding containing some percentage of aluminum. The lower thermal conductivity and diffusivity in the AlGaN claddings also favor anisotropic heat propagation in the waveguide.

A principal argument for the relatively low onset temperature of the COD mechanism is provided by the dramatic increase of absorption in the waveguide when the temperature rise in the vicinity of a defect site reduces the energy gap of the waveguide material to a value corresponding to the 450-nm emission wavelength. For GaN, this is the case at ~ 1000°C. For indium-containing material, the corresponding temperature is even lower.

Our experiments do not provide an accurate onset temperature for the COD mechanism. We show, however, that more than ~ 1000°C is not required to change the absorption of the material dramatically. Local heating at a micron-sized site by absorption of laser emission, however, easily leads to such local temperatures. Such sites might be located inside devices. Therefore, the resulting process is sometimes called catastrophic optical bulk damage.[15] In our study, the local heating begins at the front facets. The physics, however, is the same, involving interplay between increased local absorption and local temperature rise.

Damage Propagation and Comparison with GaAs-Based Devices

We also measured a "burning time" of ~ 730 ns, namely the fraction of the destructive pulse at which the power dropped substantially compared with a noncatastrophic pulse under identical conditions. Together with the length of the channel, we conclude that the hot spot must have moved from the starting point at the front facet to the endpoint of the channel with speed of about 110 μm/μs. This is substantially faster than observed earlier in comparable pulsed[18] and continuous-wave experiments[19] on GaAs-based devices.

The thermal conductivity of GaN is 2.4× higher than that of GaAs and 5.6× higher than that of $Al_{0.2}Ga_{0.8}As$, a more typical waveguide composition in AlGaAs diode lasers. Because of its higher specific heat capacity and density, the thermal diffusivity governing propagation of heat in GaN is 1.5× and 3.3× higher than that in GaAs or $Al_{0.2}Ga_{0.8}As$, respectively (see Table I). Figure 4 shows exemplary temperature profiles in

Table I. Thermal properties of relevant materials according to Refs. 16 and 17

		Unit	GaN	$Al_{0.1}Ga_{0.9}N$	AlN	GaAs	$Al_{0.2}Ga_{0.8}As$	$Al_{0.4}Ga_{0.6}As$
Thermal conductivity	λ	W/m-K	130	28	285–350	55	22.5	9.9
Density	ρ	g/cm^3	6.15	5.86	3.23	5.32	5.08	4.7
Heat capacity	C_v	J/kg-K	431–490	501	600–748	330	354	378
Thermal diffusivity	D	μm^2/μs	43	9.5	147	31	12.51	5.2
Melting point	T_m	°C	2500		3273–4800	1240	1250	1306
Melting enthalpy	H_m	kJ/g	78.5		150	39.5	–	–

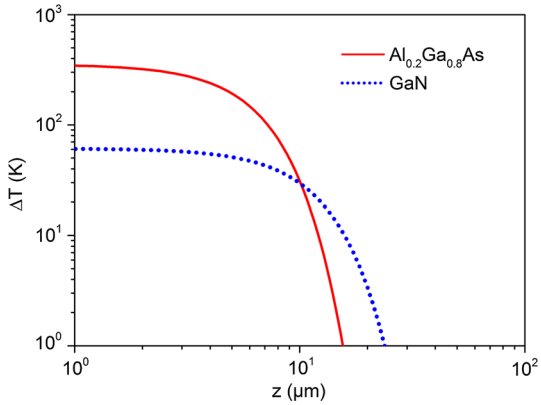

Fig. 4. Modeling of two-dimensional heat diffusion over duration of 800-ns pulse in $Al_{0.2}Ga_{0.8}As$ and GaN. The local positions (z) where the temperature reaches 50% of the maximum value at $z = 0$ are 5.3 μm and 10.1 μm for $Al_{0.2}Ga_{0.8}As$ and GaN, respectively.

homogeneous GaN and $Al_{0.2}Ga_{0.8}As$ materials 800 ns after absorbing an energy density of $Q = 0.8$ nJ/μm, a value obtained by assuming 1% absorption of the power density of 1 W/μm at the beginning of the 800-ns pulse duration. In our simplified model for a broad-area emitter, we assumed two-dimensional diffusion into the half-space away from the mirror into homogeneous waveguide material with Dirac excitation at $y = z = 0$ and $t = 0$. The thermal diffusion equation $\partial T/\partial t = D\,\Delta T$ for homogeneous media with diffusion constant $D = \lambda/\rho/C_v$, derived from the thermal conductivity λ, the specific heat C_v, and the density ρ of the material (cf. Table I), has a simple analytical solution (heat pole) which can be readily expanded to the rotationally symmetric case in 3 dimensions:

$$T = T_0 + \frac{Q}{\rho C_v} \cdot \frac{e\left(\frac{-r^2}{4Dt}\right)}{\sqrt{(4\pi Dt)^N}}, \qquad (1)$$

with $r^2 = x^2 + y^2 + z^2$. According to this simple model for homogeneous materials, the same absorbed energy would raise the local temperature 5.8 times less and diffuse 1.8 times further in GaN. If absorption at similar facet coatings and defects limits the COD threshold in both material systems, this improved conductive cooling in GaN may ultimately allow higher COD threshold intensities. The diffusion in an actual waveguide with less conductive claddings will be slower than predicted by this optimistic model for homogeneous waveguide material. It is thus clear that heat diffusion alone cannot explain the observed COD defect front propagation, in either material system.

Obviously, COD propagation in waveguides is a "fuse" effect where a thermally induced phase change is driven by the remaining mode in the intact waveguide section. Thus, in contrast to our modeling, the heat source is moving along the laser axis.

Assuming that the "missing" 2 μJ measured during the 800-ns pulse heated only a 6.5-μm-wide filament and a 400-nm-thick waveguide section of 80 μm length yields an energy density of 9.7 kJ/cm^3, which would represent 74% of the melt enthalpy, 12.8 kJ/cm^3, or a temperature rise of $\sim$ 3200 K. Considering that GaN disintegrates without melting (enthalpy) as well as some loss due to lateral diffusion from the waveguide, this measurement would be consistent with heating of some 1000 K.

The specific energy required to heat GaN to $\sim$ 1000°C, where it disintegrates, is $\sim$ 340 J/g, about 23% less than the 440 J/g needed to heat and melt GaAs. On the other hand, the higher thermal conductivity and smaller mode field in GaN-based devices would favor greater lateral diffusion loss. The ratio in thermal conductivity between a GaN waveguide and its AlGaN cladding is 4 to 5, twice that for a typical AlGaAs waveguide, which will reduce lateral diffusion and favor propagation along the waveguide direction. Overall, based on the observation that, for a 0.8-μs pulse, the fuse velocity exceeds thermal diffusion more than tenfold, we expect lateral diffusion to cool the fused channel, but contribute little to increasing the thermal cross-section of the fuse front. According to the heat pole Eq. 1, the time t until the temperature peaks a distance r from the origin is inversely proportional to the square of r, namely $t \sim r^{-2}$, allowing for nearly arbitrarily fast propagation over short distances. Heat diffusion is thus the likely mechanism, along with acoustic phonons, to carry the absorption front and fuse forward.

The faster "fuse" speed in GaN at comparable COD intensities of $\sim$ 1 W/μm^2 likely arises from

more "efficient" absorption of the remaining mode: Absorption above the bandgap reaches 10^5 cm^{-1} in GaN, ten times as much as in GaAs, concentrating the hot front with steeper gradients and thus driving faster propagation. Besides, the sharp interface to an empty channel in GaN may favor reflection of transmitted light and phonons to the hot spot, while the recrystallized AlGaAs may contribute to increased scattering loss. Clear assignment of the actually acting acceleration mechanisms, however, lies beyond the scope of this paper.

CONCLUSIONS

We investigated GaN-based diode lasers that were intentionally damaged using single sub-μs current pulses, provoking COD. Subsequently, we analyzed the related damage pattern inside the device. Surprisingly, the damage signature was an empty channel, exactly at the expected position of the optical mode. This finding is consistent with earlier observations of material ejected out of the front facet during the COD event.[12] Measurement of the resulting cavity size and the pulse power and shape allowed estimates of the energy introduced into the observed defect as well as the temperatures ($\sim$ 1000°C) reached during the process, with defect propagation velocities of 110 μm/μs.

The defect propagation velocity in GaN is 4 to 5 times higher than in GaAs-based devices. Moreover, a simple diffusion model shows that, in both cases, it is much faster than driven by diffusion alone. The propagation of the defect is a "fuse" effect where a thermally induced phase change is driven by the mode in the remaining intact waveguide.

We speculate that the much higher absorption of GaN above the bandgap, as well as its higher thermal conduction and diffusion velocity, are responsible for the faster propagation of the heated fuse front. Also, thermal runaway is likely to start at lower temperature in GaN- than GaAs-based devices, probably below 1000°C.

ACKNOWLEDGEMENTS

The authors thank Dr. Anna Mogilatenko and Dr. Harald König for helpful discussions. We also thank Dr. Elodia Musu of CRS4-Cagliari for FIB sample preparation, and Dr. Vittorio Morandi and Dr. Andrea Migliori of CNR-IMM Bologna for TEM/STEM analysis.

REFERENCES

1. C. Harder, *Pump Diode Lasers* (Amsterdam: Elsevier, 2008), p. 107.
2. J.W. Tomm, M. Ziegler, M. Hempel, and T. Elsaesser, *Laser Photon. Rev.* 5, 422 (2011).
3. M. Furitsch, *Untersuchung von Degradationsmechanismen an (Al/In)GaN-basierenden Laserdioden*, 1st ed. (Göttingen: Cuvillier, 2007), p. 168.
4. T. Schoedl, U.T. Schwarz, V. Kummler, M. Furitsch, A. Leber, A. Miler, A. Lell, and V. Harle, *J. Appl. Phys.* 97, 1231021 (2005).
5. T. Schoedl, U.T. Schwarz, S. Miller, A. Leber, M. Furitsch, A. Lell, and V. Harle, *Phys. Status Solidi A Appl. Res.* 201, 2635 (2004).
6. U. Strauss, A. Somers, U. Heine, T. Wurm, M. Peter, C. Eichler, S. Gerhard, G. Bruederl, S. Tautz, B. Stojetz, A. Loeffler, and H. Koenig, *Proc. SPIE* 10123, 101230A (2017).
7. G. Mura, M. Vanzi, M. Hempel, and J.W. Tomm, *Phys. Status Solidi (RRL) Rapid Res. Lett.* 11, 17001321 (2017).
8. H.Y. Ryu, K.H. Ha, S.N. Lee, K.K. Choi, T. Jang, J.K. Son, J.H. Chae, S.H. Chae, H.S. Paek, Y.J. Sung, T. Sakong, H.G. Kim, K.S. Kim, Y.H. Kim, O.H. Nam, and Y.J. Park, *Photon. Technol. Lett. IEEE* 18, 1001 (2006).
9. H.Y. Ryu, K.H. Ha, S.N. Lee, K.K. Choi, T. Jang, J.K. Son, H.G. Kim, J.H. Chae, H.S. Paek, Y.J. Sung, T. Sakong, K.S. Kim, O.H. Nam, and Y.J. Park, *Proc. SPIE* 6352, 63521I (2006).
10. M. Kawaguchi, H. Kasugai, K. Samonji, H. Hagino, K. Orita, K. Yamanaka, M. Yuri, and S. Takigawa, *IEEE J. Sel. Top. Quantum Electron.* 17, 1412 (2011).
11. M. Hempel, M. Ziegler, J.W. Tomm, T. Elsaesser, N. Michel, and M. Krakowski, *Appl. Phys. Lett.* 96, 251105 (2010).
12. M. Hempel, J.W. Tomm, B. Stojetz, H. König, U. Strauss, and T. Elsaesser, *Semicond. Sci. Technol.* 30, 0720011 (2015).
13. S. Porowski, B. Sadovyi, S. Gierlotka, S.J. Rzoska, I. Grzegory, I. Petrusha, V. Turkevich, and D. Stratiichuk, *J. Phys. Chem. Solids* 85, 138 (2015).
14. W. Utsumi, H. Saitoh, H. Kaneko, T. Watanuki, K. Aoki, and O. Shimomura, *Nat. Mater.* 2, 735 (2003).
15. Y. Sin, Z. Lingley, M. Brodie, N. Presser, and S.C. Moss, *Proc. SPIE* 10086, 100860S1 (2017).
16. http://www.ioffe.ru/SVA/NSM/Semicond/.
17. V.P. Vasil'ev and J.C. Gachon, *Inorg. Mater.* 42, 1176 (2006).
18. M. Hempel, F. La Mattina, J.W. Tomm, U. Zeimer, R. Broennimann, and T. Elsaesser, *Semicond. Sci. Technol.* 26, 075020 (2011).
19. J.H. Jacob, R. Petr, M.A. Jaspan, S.D. Swartz, M.T. Knapczyk, and A.M. Flusberg, *Proc. SPIE* 7198, 7198151 (2009).